Solid-state reactivity explored *in situ* by synchrotron radiation on single crystals: from $SrFeO_{2.5}$ to $SrFeO_3$ via electrochemical oxygen intercalation

2015 J. Phys. D: Appl. Phys. 48 504004

(http://iopscience.iop.org/0022-3727/48/50/504004)

OPEN ACCESS
IOP Publishing
Journal of Physics D: Applied Physics
J. Phys. D: Appl. Phys. **48** (2015) 504004 (14pp)
doi:10.1088/0022-3727/48/50/504004

Solid-state reactivity explored *in situ* by synchrotron radiation on single crystals: from $SrFeO_{2.5}$ to $SrFeO_3$ via electrochemical oxygen intercalation*

A Maity[1], R Dutta[1,2], B Penkala[1], M Ceretti[1], A Letrouit-Lebranchu[1], D Chernyshov[3], A Perichon[1], A Piovano[4], A Bossak[5], M Meven[6] and W Paulus[1]

[1] Institut Charles Gerhardt, UMR 5253, CNRS-Université de Montpellier, 34095 Montpellier, France
[2] Paul-Scherrer-Institut, LNS, 5232 Villigen, Switzerland
[3] Swiss-Norwegian Beamlines at the European Synchrotron Radiation Facility, 38000 Grenoble, France
[4] Institut Laue-Langevin, 71 avenue des Martyrs, 38000 Grenoble, France
[5] European Synchrotron Radiation Facility, 38000 Grenoble, France
[6] Institut für Kristallographie, RWTH Aachen and Jülich Centre for Neutron Science (JCNS) at Heinz Maier-Leibnitz Zentrum (MLZ), Lichtenbergstraße 1, 85748 Garching, Germany

E-mail: werner.paulus@univ-montp2.fr

Received 29 June 2015, revised 21 August 2015
Accepted for publication 7 September 2015
Published 1 December 2015

Abstract

In this study we demonstrate the feasibility of following up a chemical reaction by single crystal x-ray (synchrotron) diffraction under *operando* conditions, carried out in a specially designed electrochemical cell mounted on the BM01A at the European Synchrotron Radiation Facility (ESRF). We investigated in detail the electrochemical oxidation of $SrFeO_{2.5}$ to $SrFeO_3$ on a spherical single crystal of 70 μm diameter by *in situ* diffraction at an ambient temperature. Complete data sets were obtained by scanning the whole reciprocal space using a 2M Pilatus detector, resulting in 3600 frames with a resolution of 0.1° per data set, each obtained in 18 min. The crystal was mounted in a specially designed electrochemical cell with 1N KOH used as the electrolyte. During the electrochemical oxidation, the reaction proceeds following the phase sequence $SrFeO_{2.5}/SrFeO_{2.75}/SrFeO_{2.875}/SrFeO_3$, structurally accompanied by establishing a complex series of long-range oxygen vacancy ordering, which gets instantly organized at ambient temperature. The topotactic reaction pathway is discussed in terms of the evolution of the twin domain structure. The formation of $SrFeO_{2.875}$ is accompanied by the formation of diffuse streaks along the [1 0 0]-direction of the perovskite cell, reaching high *d*-spacings. The diffuse streaks are discussed and are thought to originate from a modified twin structure induced by the $SrFeO_{2.75}$ to $SrFeO_{2.875}$ transition, and the associated changes in the domain structure, developed during the oxygen intercalation. We equally analysed and discussed in detail the twin structure of all the title compounds. We confirm the ground state of $SrFeO_{2.5}$ is able to adopt the *Imma* space group symmetry, showing stacking faults of the tetrahedral layers along the stacking axis of the brownmillerite unit cell, indicated by the 1D diffuse rods. We showed that *in situ* single crystal diffraction has huge potential in the study of non-stoichiometric compounds under *operando* conditions, in order to obtain structural information i.e. about diffuse scattering, and microstructural information related to domain effects such as twinning—information far beyond that which powder diffraction methods allow us to obtain.

* Dedicated in honour of Professor Robert Schöllhorn on the occasion of his 80th birthday.

Keywords: *in situ* diffraction, non-stoichiometric oxides, synchrotron radiation, diffuse scattering, twinning, chemical reactivity of solids, electrochemistry

S Online supplementary data available from stacks.iop.org/JPhysD/48/504004/mmedia

(Some figures may appear in colour only in the online journal)

1. Introduction

Due to the high performance of modern x-ray and neutron diffractometers, the chemical reactivity of solids is studied today routinely under *in situ* conditions on polycrystalline samples in specific reaction chambers [1–4]. This technique became the standard characterization not only for battery systems but also for catalysis and many other applications. Following up chemical solid-state reactions on single crystals would be even more powerful, as it would allow for scanning of the whole reciprocal lattice. This would allow us to obtain valuable information about diffuse scattering and weak superstructure reflections, as well as gather information about the volume fraction of different domains during the reaction, to highlight a few examples which are difficult or impossible to access by powder diffraction. In spite of all these benefits, solid-state reactivity followed up on single crystals, is almost unreported in literature and is generally limited to surface reactions or defined starting and final reaction products [5, 6]. The main reasons for this are related to the reaction kinetics, which usually leads to inhomogeneous samples, especially for larger grain sizes becoming difficult to quantify; other reasons concern the related structural complexity, as any type of disorder, twinning, stacking faults or domain effects usually demand sophisticated and time-consuming data analysis.

Recent developments concerning fast and low-noise 2D-detectors, together with a high primary beam quality, developments which are especially available at large scale facilities but also via μ-focus type x-ray sources using standard laboratory equipment, present huge potential in the study of solid-state reactivity on single crystals of a sufficiently low size on a reasonable timescale under equilibrium conditions. The single crystal diffractometer BM01A installed at the Swiss–Norwegian beamline at the European Synchrotron Radiation Facility (ESRF) perfectly combines rapid data collection using a 2D Pilatus detector, with a high quality beam without harmonics, and is thus ideally suited to study single crystals of several microns in a reasonable timescale [7].

We report here on the electrochemical oxygen intercalation reaction into $SrFeO_{2.5}$ single crystals, followed up *in situ* by x-ray diffraction in a dedicated, miniaturized electrochemical cell, which was mounted on the BM01A goniometer. We were especially interested to structurally explore the phase diagram of $SrFeO_{3-x}$ at ambient temperature, as it is interesting from a crystal chemistry point of view; in addition all involved phases have interesting magnetic properties, and their performance concerning low temperature oxygen mobility has potential interest in terms of energy storage and conversion. We equally focused on the formation mechanisms of all involved phases and specifically on the two intermediate phases $SrFeO_{2.75}$ and $SrFeO_{2.875}$, which have been reported as line phases, and up to which extent the oxygen intercalation reaction pathway proceeds topotactically.

2. Experimental procedure

Single crystals of $SrFeO_{2.5}$ have been grown by the floating zone method. To this end polycrystalline $SrFeO_{2.5}$ was first prepared using standard solid-state chemistry methods. High purity $SrCO_3$ (99.95%) and Fe_2O_3 (99.99%) were thoroughly mixed and then heated in air at 1000 °C for 24 h. After being furnace-cooled to room temperature, the obtained product was ground and pressed into pellets of approximately one g each. The pellets were then sintered at 1200 °C for 24 h, and subsequently quenched in air down to ambient temperature. Seed and feed rods for crystal growth were obtained by hydrostatic pressing of the $SrFeO_{2.5}$ powder at 10 bars in a cylindrical latex tube of 8 mm in diameter and 150 mm in length. The obtained rods were then sintered in air at 1200 °C for 24 h to obtain dense polycrystalline rods.

Single-crystal growth was carried out in an optical mirror furnace (NEC SC2, Japan) equipped with two 500 W halogen lamps as a heat source and two ellipsoidal mirrors [8]. Crystal growth was performed in a high-purity Ar-atmosphere (99.999%) with a typical traveling rate of 1–2 mm h^{-1}, while the upper and lower shafts were rotated in opposite directions at 35 rpm similar to [9]. The obtained grown crystals had a typical length of up to 10 cm and 8 mm in diameter, and a shiny metallic lustre. A photo of a typically obtained crystal is shown in figure S1 in the supplementary part of this paper (stacks.iop.org/JPhysD/48/504004/mmedia). From the grown crystal a 70 μm thick spherical crystal was obtained for the *in situ* experiment by manual liming.

The electrochemical cell used for this *in situ* study, allows us to dispose the same liberties of movements for single crystal diffraction as for a standard goniometer head(see figure 1). It essentially consists of two quartz glass Debye–Scherrer capillaries with different diameters (0.3 and 0.7 mm), which were telescoped, while the inner capillary was used to mount a 50 μm thick gold wire on top of which the crystal was glued with a silver paste. The 1N KOH electrolyte was steadily pumped through the inner capillary, which was cut at its end position, while flowing back through the outer one. A permanent electrolyte flow guaranties constant reaction conditions, but assures also the transport of oxygen bubbles, which are always

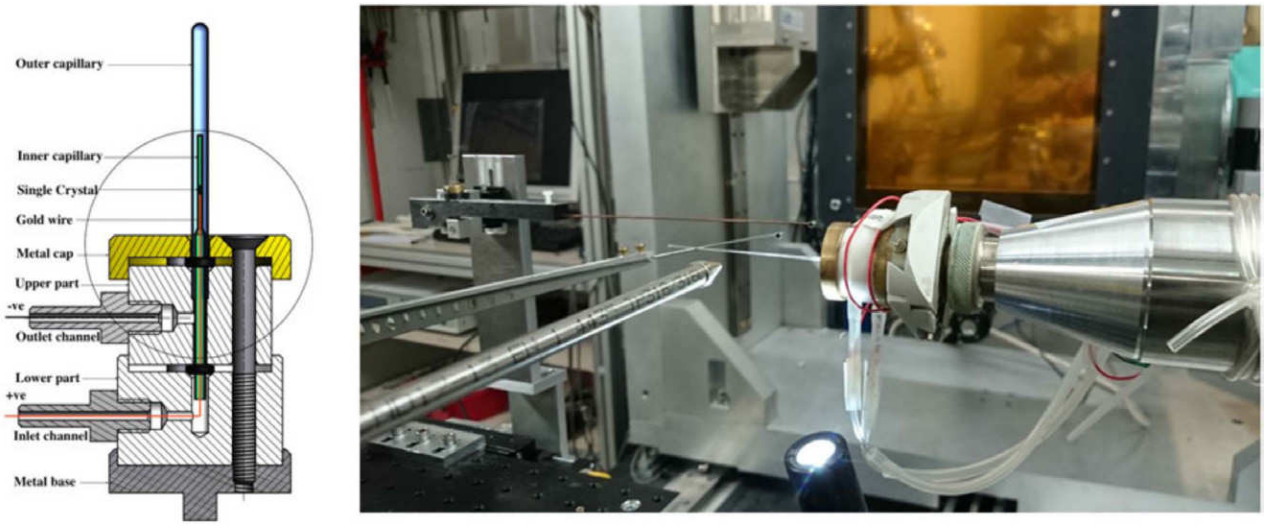

Figure 1. Assembly drawing (left) and experimental setup (right) of the electrochemical cell used for *in situ* single crystal diffraction studies during the electrochemical oxidation of a $SrFeO_{2.5}$ single crystal on BM01A. The whole cell allows free rotation of 360°, enabling us to scan an important part of the whole reciprocal space, suitable for the reconstruction of specific lattice planes.

produced as a by-product during the electrolysis, away from the crystal. A constant current of 10 μA was applied during the whole intercalation reaction.

Monitoring the on-going intercalation reaction on BM01A, strongly benefits the fast and almost zero noise data collection, which is possibly due to the combination of a sufficiently high beam intensity together with the use of a 2M Pilatus detector, having a readout time of 2.5 ms only. The detector was energetically tuned to widely suppress any fluorescence below 12.00 keV, and especially originating from Fe (K-absorption edge at 7.112 kV with K_α at 6.403 keV and K_β at 7.06 keV) while for Sr no fluorescence problem existed for the wavelength used, corresponding to exactly 16.00 keV, the Sr absorption edge being at 16.104 keV. An important advantage of BM01A in terms of unambiguous data interpretation, is the absence of contaminations by harmonics and its very narrow energy resolution, achieved via a combination of focusing beam optics with a double crystal monochromator. Data was collected in a timescale of 0.3 s per frame while rotating the electrochemical cell with a 0.1° angular step. A full sphere data collection takes 18 min for 3600 frames. Data collection was done perpetually, allowing us to register a total of 1.188.000 frames during 5 d, presenting a data size of 2.7 TB. The wavelength used for the whole experiment was $\lambda = 0.7750$ Å.

The data was pre-processed with the SNBL (Swiss–Norwegian beamlines) ToolBox (Diadkin 2015); reflection indexing and inspection of the reciprocal space was done with CrysAlis software (version 171.31.35).

Details concerning the specificities of BM01A can be found under [7].

3. Results and discussion

3.1. Correlation of structure and non-stoichiometry in $SrFeO_{3-x}$

$SrFeO_{3-x}$ is a complex oxide, allowing a variation of the oxygen stoichiometry between $0 \leqslant x \leqslant 1$. Investigated for more than five decades [10–15], it combines structural complexity together with interesting physical properties, especially concerning magnetism [16–22]. While reversible oxygen uptake and release is observed for $0 \leqslant x \leqslant 0.5$, the lower end member $SrFeO_2$ with $x = 1$, can only be obtained by low temperature reduction using the CaH_2 method and adapts the infinite layer structure [23]. Two intermediate phases $SrFeO_{2.75}$ and $SrFeO_{2.875}$ have been reported as line phases [24–26], showing a more complex magnetic and structural ordering. $SrFeO_{3-x}$ belongs to the few systems where the oxygen stoichiometry can not only be adjusted at elevated temperatures under controlled oxygen partial pressure [27], but which can be electrochemically oxidized or reduced between $0 \leqslant x \leqslant 0.5$ already at ambient temperature in a reversible topotactic reaction [26]. The reaction can be described by the following reaction equation:

$$SrFeO_{2.5} + x\ O^{2-} \rightleftarrows SrFeO_{2.5+x} + 2x e^- \qquad (1)$$

Applying a constant current, the reaction velocity and thus the kinetics can be principally controlled in a galvanostatic way, also allowing us to precisely adjust the oxygen stoichiometry. Thereby oxygen is intercalated into the 1D vacancy channels of the $SrFeO_{2.5}$ brownmillerite type structure, changing the coordination of Fe from octahedral/tetrahedral to purely octahedral for the $SrFeO_3$ framework. As indicated in figure 2, the intermediate phases $SrFeO_{2.75}$ and $SrFeO_{2.875}$ show octahedral geometry together with square pyramidal oxygen coordination of Fe.

The oxidation of the $SrFeO_{2.5}$ brownmillerite phase to the cubic $SrFeO_3$ phase with perovskite-type structure has already been investigated by *in situ* x-ray powder diffraction and the samples at different charge transfer rates have been studied *ex situ* by TEM and Mössbauer spectroscopy [26]. While no intermediate phase could have been observed by powder x-ray diffraction, $SrFeO_{2.75}$ and $SrFeO_{2.875}$ have been identified by more local methods such as TEM and Mössbauer spectroscopy. Since phase identification and separation in $SrFeO_{3-x}$ for $x = 0$, 0.125, 0.25 and 0.5 should in principle be feasible with powder x-ray diffraction, the obtained results in [26] suggest the formation of small domains during the oxidation reaction are difficult to detect; this issue is related to the coherence problem of

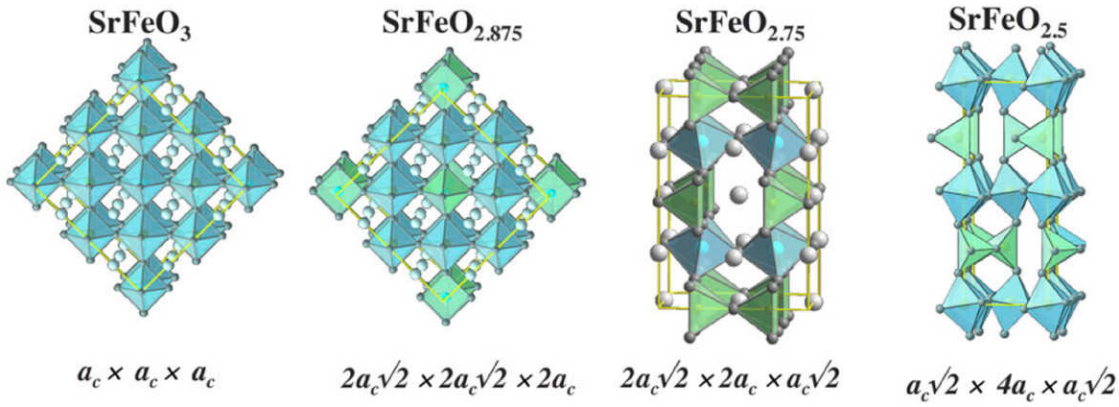

Figure 2. $SrFeO_{3-x}$ phases showing long-range oxygen vacancy ordered superstructures with Fe in octahedral, square pyramidal and tetrahedral coordinations. The unit cell dimensions are given with respect to the cubic parent perovskite structure.

Table 1. Phases and related symmetries and lattice parameters for the $SrFeO_{3-x}$ system taken from [27].

Phase	Space group	Lattice parameters (Å)
$SrFeO_{2.5}$	*Imma*	*a*: 5.527(1)
		b: 15.59(2)
		c: 5.672(1)
$SrFeO_{2.75}$	*Cmmm*	*a*: 10.974(1)
		b: 7.702(1)
		c: 5.473 (1)
$SrFeO_{2.875}$	*I4/mmm*	*a*: 10.929(1)
		c: 7.698(1)
$SrFeO_3$	*Pm*-3*m*	*a*: 3.851(1)

nano-domains. While TEM has indeed a much shorter coherence length compared to x-ray diffraction, it might be a very powerful tool for the phase characterization of non-stoichiometric oxides, provided they are stable in a vacuum under the reducing conditions. This is the case for $SrFeO_{2.5}$, though this is more difficult for $SrFeO_{2.75}$ and $SrFeO_{2.875}$, due to the easy oxygen release under the vacuum and reducing conditions.

The established phase diagram as reported in [27] shows four distinct phases and related lattice parameters as summarized in table 1.

Although all basic structure frameworks of the phases presented in figure 2 have been known for a long time, some of them are still under debate regarding subtle but important details; this is even true for $SrFeO_{2.5}$ which shows a brownmillerite-type structure.

This phase has been described as showing a disordered tetrahedral layer sequence, crystallizing in the *Imma* space group [16]; it has been recently reported to show an ordered FeO_4 tetrahedra chain arrangement at ambient temperature with a doubling of the axis perpendicular to the $(FeO_4)_\infty$ chain direction. This occurs in conjunction with an increase of the two crystallographically different Fe sites present in *Imma,* to four Fe sites present in *Pbma*, contradictory to what has been reported before from Mössbauer spectroscopy and neutron diffraction studies [28, 29]. High resolution TEM investigations on $SrFeO_{2.5}$ revealed instead a perfect ordering of adjacent $(FeO_4)_\infty$ chains within a given tetrahedral layer, while different types of stacking faults of the (FeO_4) tetrahedral layers along the stacking axis give rise to 1D rows of diffuse intensities running along the *b*-axis of the brownmillerite framework [30], still with *Imma* as the underlying space group. In detail the structure has been described in the (3 + 1)-dimensional superspace group $I2/m(0\beta\gamma)0s$, $\boldsymbol{q} = \beta\mathbf{b}^* + \gamma\mathbf{c}^*$, $0 \leqslant \beta \leqslant ½$ and $0 \leqslant \gamma \leqslant 1$. As will be shown below, these diffuse rods appear as regular reflections on superstructure reflection positions for special projections related to the twin domain structure, as is the case when looking along [*010*] in the average brownmillerite *Imma* structure (see figures 6 and 7). The stacking disorder has been simulated successfully and intergrowth phases related to a stacking sequence with C2/m or Pbma space group could have been identified [30]. The degree of stacking disorder has been interpreted to depend on the history of the crystallites, identifying TEM as a very powerful tool to quantitatively describe stacking disorder in solids. Before discussing the results obtained during the electrochemical oxidation of $SrFeO_{2.5}$, we first investigate up to which extent its real structure can be accessed with single crystal synchrotron diffraction.

3.2. The ground state of $SrFeO_{2.5}$

The real structure of $SrFeO_{2.5}$ presents an important issue, as it does not only concern its structure and symmetry but equally its lattice dynamical aspects. The latter have been discussed controversially in terms of phonon assisted diffusion, which has already been achieved at around 310 K [31–36] in the disordered structure with the *Imma* space group. Following [29], discussion suggests that O-mobility sets in at 813 K only; this is related to a *Pbma* to *Imma* phase transition, due to confined local rotations of the FeO_4 tetrahedra.

We consequently investigated the structure of $SrFeO_{2.5}$ at ambient temperature on BM01A on the same crystal, prior to the *in situ* experiments. We note that the parent structure of $SrFeO_{3-x}$ under crystal growth conditions at high temperature is cubic, while it transforms to the orthorhombic brownmillerite structure slightly below 1173 K [12]. This phase transition is unavoidable, accompanied by the formation of twin domains as further outlined below. Related to the number of possible twin individuals, the reconstructed lattice planes appear at first sight to be rather complex. The crystal used for the experiment has been chosen, as it presents only four

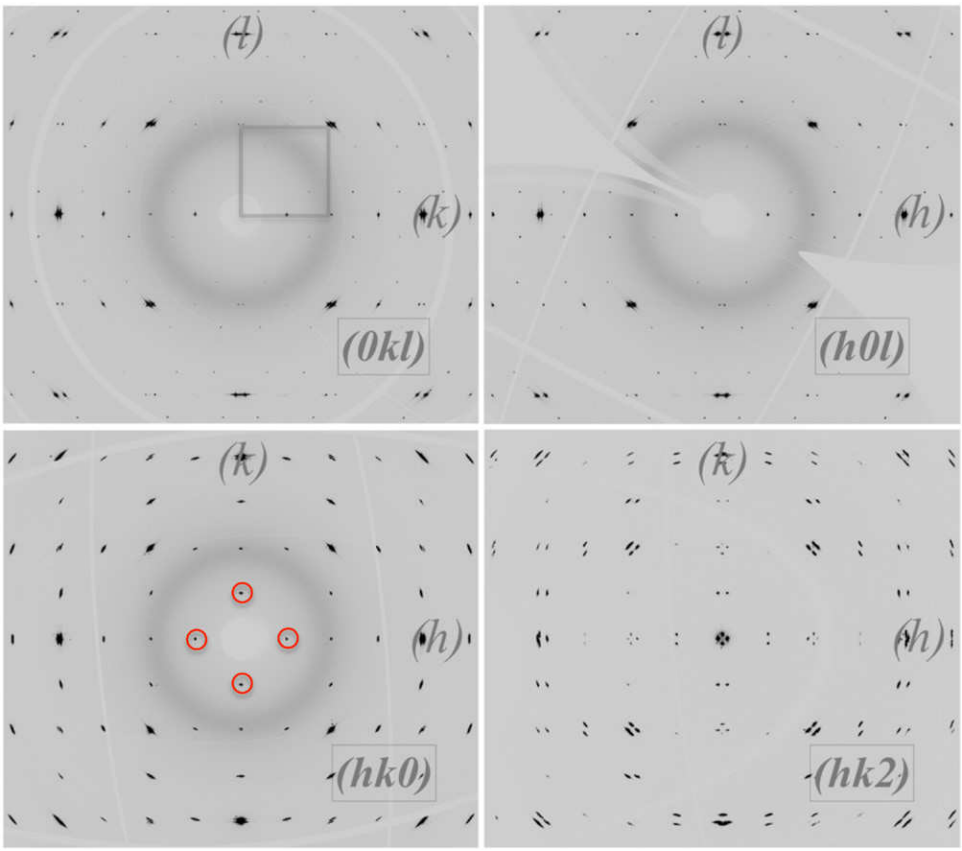

Figure 3. Reconstruction of the (*0kl*), (*h0l*) *and* (*hk0*) planes with respect to the parent cubic perovskite cell, outlined as a grey square for the (*0kl*)-plane. The presence of only two equivalent (*½00*)-type reflections in the (*0kl*) and (*h0l*) planes (appearing together in the (*hk0*) plane) with a *d*-spacing of 7.79 Å (red circles) indicate that only two out of three possible orientation variants of the brownmillerite unit cell with *b*-axes running along the three principal axes of the perovskite cell are present (see figure 4(c)); for each of them two out of four twin individuals are observed, as indicated from the splitting behaviour of the (*001*)-type perovskite reflections. No splitting of any (*hkl*) reflections is detectable in the (*hk0*) plane, as the reflections of different individuals are separated in higher order planes. Small separations in the reflection positions are related here for different ***q*** values only as a result of the domain overlay via twinning. From the (*hk2*)-plane it becomes evident that the four twin individuals are separated along the *l*-direction. In total only four twin domains out of twelve possible ones are present, clearly separated for the (*0kl*) *and* (*h0l*) as well as in the (*hk2*) planes. We note the (*100*) and (*010*) planes are the common twin planes for both sets of twin individuals respectively.

out of 12 twin domains, allowing a less complex data analysis compared to the presence of 12 twin domains. It should thus allow us to obtain information about the reaction mechanism and diffusion pathway, which is not possible from powder diffraction.

Figure 3 shows the reconstructed (*hk0*), (*0kl*) and (*h0l*) planes with respect to the small cubic perovskite cell. One can immediately observe that they are not equivalent in symmetry; this is related to the twinning. In the following we therefore first introduce the twin behaviour, allowing us finally to conclude on the structural evolution, especially with respect to a topotactic oxygen reaction pathway.

The twinning behaviour can be understood easily, considering the long stacking *b*-axis of the brownmillerite unit cell to run along the principal *a*-, *b*- and *c*-axes of the parent perovskite unit cell, while the *a*- and *c*-axes are oriented along its [*110*]-type directions (see figure 4(c) [37, 38]. Related to the fact that the *a*- and *c*- lattice parameters differ slightly, a pseudo-merohedric twin scheme as outlined in figures 4(a) and (b) is presented, showing the common twin planes (*101*) and (*-101*), and finally resulting in up to four possible twin domains related to one common *b*-axis. The spatial separation of (*h00*) reflections is given by:

$$\Delta = \arctan(a/c) - \arctan(c/a) \tag{2}$$

and thus directly providing information on the orthorhombicity [37]. Resuming, the number of all possible twin domains mounts up to a maximum of 12, in the case of the presence of three *b*-axis oriented brownmillerite unit cells, each showing up to four domains respectively. The matrices relating all individuals are given in table 2.

A closer inspection of the three equivalent (*hk0*)-type planes reveals the presence of only two (*0½0*)-type reflections with a *d*-spacing of 7.79 Å, corresponding to the (*020*) reflection of the brownmillerite structure in *Imma*. Each (*020*) reflection present, indicates the *b*-axis orientation of one brownmillerite unit cell and allows consequently the appearance of up to four twin individuals; these are then spatially separated in the (*a, c*)-plane as all twinning is pseudo-merohedric, following the twin laws outlined in figures 4(a)–(c) and table 2.

A detailed analysis shows the presence of four twin domains in total for the whole crystal, while a common *b*-axis

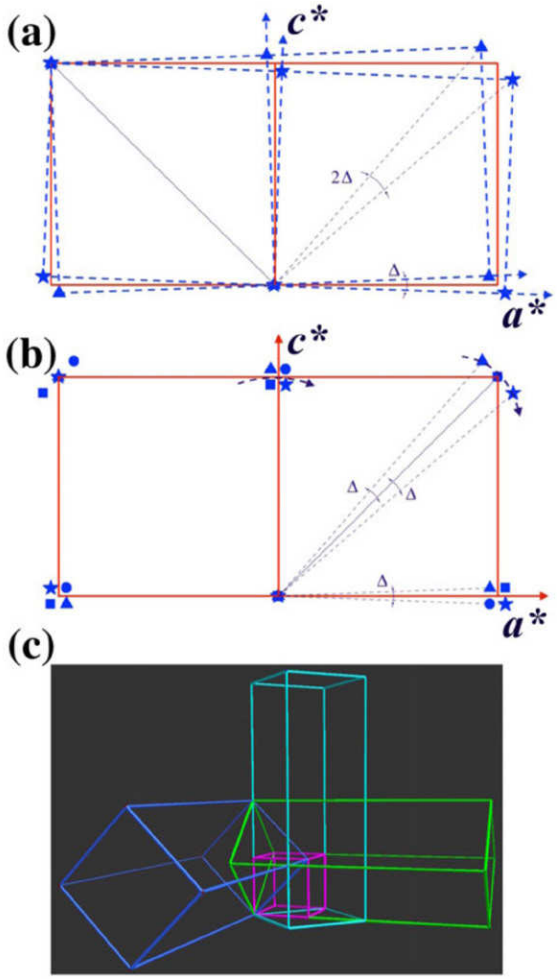

Figure 4. Twin scheme for a tetragonal-orthorhombic phase transition, with the common (*101*) twin plane (top), resulting in up to four twin individuals when the equivalent (*-101*) twin plane is added. The parent tetragonal unit cell is outlined in red, and the (*hkl*) indexing refers to the *b*-axis as the tetragonal axis, in order to be directly comparable with the brownmillerite unit cell. The spatial separation of the reflection of the different twin domains Δ, i.e. the orthorhombicity is given by $\Delta = \arctan(a/c) - \arctan(c/a)$. The three orientation variants of the orthorhombic $\boldsymbol{a}\sqrt{2} \times 4\boldsymbol{a} \times \boldsymbol{a}\sqrt{2}$ brownmillerite framework (green, blue and turquoise) with respect to the cubic $\boldsymbol{a} \times \boldsymbol{a} \times \boldsymbol{a}$ perovskite unit cell (pink) is given in figure 4(c). The *b*-axes of the different twin individuals are oriented along the principal axis of the perovskite cell, having a length of four $\boldsymbol{a}$. While the *a*- and *c*-axes of the brownmillerite unit cell slightly differ, twinning becomes pseudo-merohedric and the total number of twin individuals is three times four, i.e. 12 at the maximum, according to the twin scheme discussed above.

Table 2. Transformation matrices to relate the (*hkl*) values, indexed in the pseudo-cubic perovskite structure, to the specific twin individuals for the different compounds.

$SrFeO_{2.5}$

$$\begin{pmatrix} h \\ k \\ l \end{pmatrix}_{SrFeO_{2.5}} = (M) \times \begin{pmatrix} h \\ k \\ l \end{pmatrix}_{cubic}$$

$$\begin{pmatrix} 1 & 0 & -1 \\ 0 & 4 & 0 \\ 1 & 0 & 1 \end{pmatrix}; \begin{pmatrix} 1 & 0 & 1 \\ 0 & -4 & 0 \\ 1 & 0 & -1 \end{pmatrix}; \begin{pmatrix} 1 & 0 & -1 \\ 0 & -4 & 0 \\ 1 & 0 & 1 \end{pmatrix}; \begin{pmatrix} 1 & 0 & 1 \\ 0 & 4 & 0 \\ 1 & 0 & -1 \end{pmatrix}$$

$$\begin{pmatrix} 0 & -1 & 1 \\ 4 & 0 & 0 \\ 0 & 1 & 1 \end{pmatrix}; \begin{pmatrix} 0 & 1 & 1 \\ -4 & 0 & 0 \\ 0 & -1 & 1 \end{pmatrix}; \begin{pmatrix} 0 & -1 & 1 \\ -4 & 0 & 0 \\ 0 & 1 & 1 \end{pmatrix}; \begin{pmatrix} 0 & 1 & 1 \\ 4 & 0 & 0 \\ 0 & -1 & 1 \end{pmatrix}$$

$$\begin{pmatrix} -1 & 1 & 0 \\ 0 & 0 & 4 \\ 1 & 1 & 0 \end{pmatrix}; \begin{pmatrix} 1 & 1 & 0 \\ 0 & 0 & -4 \\ -1 & 1 & 0 \end{pmatrix}; \begin{pmatrix} -1 & 1 & 0 \\ 0 & 0 & -4 \\ 1 & 1 & 0 \end{pmatrix}; \begin{pmatrix} 1 & 1 & 0 \\ 0 & 0 & 4 \\ -1 & 1 & 0 \end{pmatrix}$$

$SrFeO_{2.75}$

$$\begin{pmatrix} h \\ k \\ l \end{pmatrix}_{SrFeO_{2.75}} = (M) \times \begin{pmatrix} h \\ k \\ l \end{pmatrix}_{cubic}$$

$$\begin{pmatrix} 2 & 0 & -2 \\ 0 & 2 & 0 \\ 1 & 0 & 1 \end{pmatrix}; \begin{pmatrix} 2 & 0 & 2 \\ 0 & -2 & 0 \\ 1 & 0 & -1 \end{pmatrix}; \begin{pmatrix} 2 & 0 & -2 \\ 0 & -2 & 0 \\ 1 & 0 & 1 \end{pmatrix}; \begin{pmatrix} 2 & 0 & 2 \\ 0 & 2 & 0 \\ 1 & 0 & -1 \end{pmatrix}$$

$$\begin{pmatrix} 0 & -2 & 2 \\ 2 & 0 & 0 \\ 0 & 1 & 1 \end{pmatrix}; \begin{pmatrix} 0 & 2 & 2 \\ -2 & 0 & 0 \\ 0 & -1 & 1 \end{pmatrix}; \begin{pmatrix} 0 & -2 & 2 \\ -2 & 0 & 0 \\ 0 & 1 & 1 \end{pmatrix}; \begin{pmatrix} 0 & 2 & 2 \\ 2 & 0 & 0 \\ 0 & -1 & 1 \end{pmatrix}$$

$$\begin{pmatrix} -2 & 2 & 0 \\ 0 & 0 & 2 \\ 1 & 1 & 0 \end{pmatrix}; \begin{pmatrix} 2 & 2 & 0 \\ 0 & 0 & -2 \\ -1 & 1 & 0 \end{pmatrix}; \begin{pmatrix} -2 & 2 & 0 \\ 0 & 0 & -2 \\ 1 & 1 & 0 \end{pmatrix}; \begin{pmatrix} 2 & 2 & 0 \\ 0 & 0 & 2 \\ -1 & 1 & 0 \end{pmatrix}$$

$SrFeO_{2.875}$

$$\begin{pmatrix} h \\ k \\ l \end{pmatrix}_{SrFeO_{2.875}} = (M) \begin{pmatrix} h \\ k \\ l \end{pmatrix}_{cubic}$$

$$\begin{pmatrix} 2 & 2 & 0 \\ -2 & 2 & 0 \\ 0 & 0 & 2 \end{pmatrix}; \begin{pmatrix} 2 & 2 & 0 \\ -2 & 2 & 0 \\ 0 & 0 & -2 \end{pmatrix}$$

$$\begin{pmatrix} 0 & 2 & 2 \\ 0 & -2 & 2 \\ 2 & 0 & 0 \end{pmatrix}; \begin{pmatrix} 0 & 2 & 2 \\ 0 & -2 & 2 \\ -2 & 0 & 0 \end{pmatrix}$$

$$\begin{pmatrix} 2 & 0 & 2 \\ 2 & 0 & -2 \\ 0 & 2 & 0 \end{pmatrix}; \begin{pmatrix} 2 & 0 & 2 \\ 2 & 0 & -2 \\ 0 & -2 & 0 \end{pmatrix}$$

Note: The number of twin domains is 12 for the orthorhombic phases $SrFeO_{2.5}$ and $SrFeO_{2.75}$, and decreases to six for the general case of tetragonal symmetry, while it gets reduced to three domains in $SrFeO_{2.875}$ related to the centrosymmetric *I4/mmm* space group. While the matrices above are useful to transform reflections indexed in the perovskite unit cell to the specific twin individuals of the respective phases, the $4\boldsymbol{a} \times 4\boldsymbol{a} \times 4\boldsymbol{a}$ pseudo-cubic perovskite supercell allows us to index all reflections of all individuals with integer values, regardless of which twin orientation it refers to. The transformation matrices using the $4\boldsymbol{a} \times 4\boldsymbol{a} \times 4\boldsymbol{a}$ cell are given in table S1 of the supplementary information (stacks.iop.org/JPhysD/48/504004/mmedia).

exists for each of the two sets of the two twin domains. Two twin sets as shown in figure 4(a) are thus present here. As seen in figure 5, we find in addition to the basic perovskite reflections (blue rings) also those which belong to the brownmillerite type structure (yellow rings) for different twin individuals. In addition to this, superstructure reflections (green rings) with (*0¼¾*)-type indexing become visible. These are sharp reflections at first sight and they turn out to be 1D diffuse rods as illustrated in figures 6 and 7, related to stacking faults of the tetrahedral layers, as outlined above [30]. The diffuse rods vary in intensity and periodicity as a function of the sample history.

We determined the separation of (*00l*) reflections as represented in figure 5, to be approximately 3.1° (2Δ in equation (2)), resulting from only two twin domains. This is very close to the calculated values being 2.96° and confirms

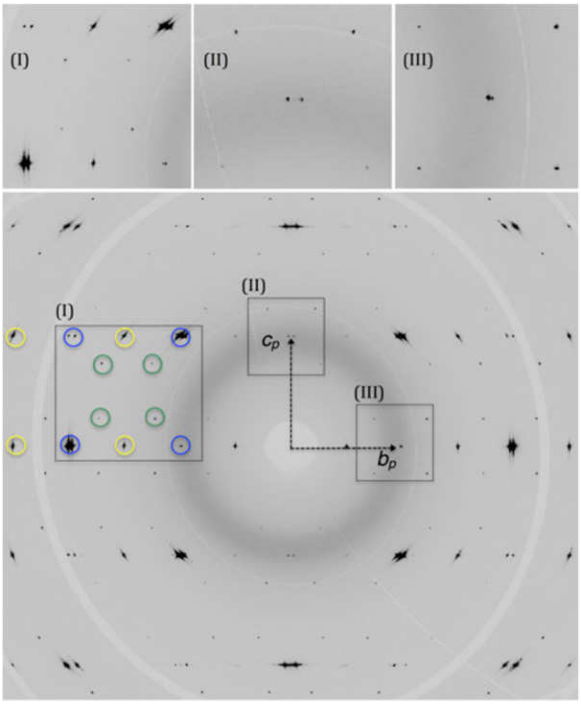

Figure 5. Reconstructed (*0kl*)-plane of $SrFeO_{2.5}$ obtained from the *in situ* diffraction experiment. The average cubic perovskite unit cell (b_p, c_p) is outlined. Blue, yellow and green rings correspond to the basic reflections of the perovskite cell, the brownmillerite and superstructure reflections; the latter presented diffuse rods running perpendicular to this plane (see figure 6). Section (I) shows the different reflection types separately. Sections (II) and (III) show a zoomed view of the (*001*) and (*010*) reflections of the perovskite cell. The splitting of the (*001*) reflection is related to the twinning outlined in figure 4, indicating that for this orientation of the brownmillerite cell, two out of four twin individuals exist, which are separated by 2Δ. Note that the (*001*)-type reflections are split horizontally and vertically, yielding four in total, i.e. 2 × (*h0h*)- and 2 × (*0hh*)-type reflections of the brownmillerite with the same *d*-spacing, e.g. as projected on the given (*hk2*) plane for the (*202*) and (*022*)-reflections in figure 3.

the twin relations discussed above. In contrast to this, we were, however, unable to identify any superstructure reflections related to the model in *Pbma* with ordered $(FeO_4)_\infty$ tetrahedral chains as related to a doubling of the *a*-axis (equal to the *c*-axis in *Pcmb* which is the equalsetting when comparing with *Imma*), and we could not reproduce the results as presented by [28], although several crystals under different growth and post-annealing conditions have been analysed.

Importantly, this implies that the ground state of $SrFeO_{2.5}$ is not adapting an ordered structure in *Pbma*, but must instead be described in *Imma*, while stacking faults are present as indicated by the diffuse rods, running along the *b*-axis of the brownmillerite unit cell. This is clearly demonstrated in figure 6, where in the (*hk¼*) plane only diffuse rods are present in two directions, due to the fact that only two twin sets, showing a common *b*-axis, are present. The diffuse rods are running along the respective *b*-axes of the different brownmillerite orientation variants.

For clarity we also compared in figure 7 the results obtained here from x-ray diffraction on BM01A to the results obtained from TEM, as published in [30]. While both projections with

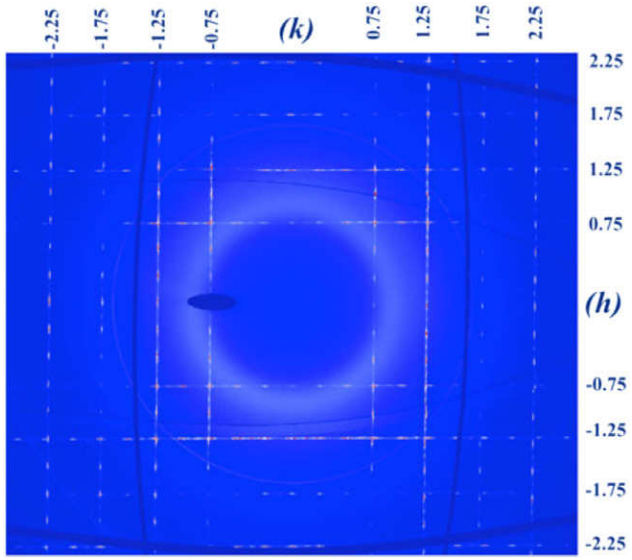

Figure 6. Reconstructed (*hk¼*) plane of the $SrFeO_{2.5}$ crystal, indexed in terms of the cubic perovskite cell. The diffuse rods result from stacking faults for two sets of twin individuals, having a common *b*-axis ($4\mathbf{a_p}$), pointing along the *a*- and *b*-axis of the perovskite cell. Contrary to the two other equivalent planes (*h¼l*) and (*¼kl*), this plane does not show any reflections related to the brownmillerite framework. For this reason this specific plane is interesting especially concerning its evolution with the oxygen content; this becomes important when concluding on the topotactic intercalation mechanism related to the intermediate phases $SrFeO_{2.75}$ and $SrFeO_{2.875}$ as shown in figures 8 and 10.

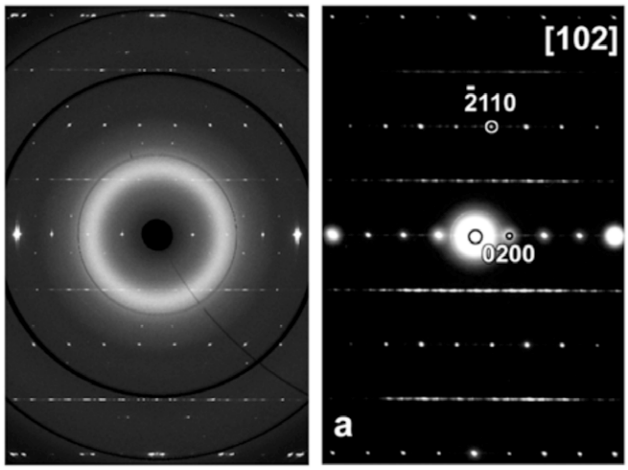

Figure 7. Comparison of the scattering planes with the zone axis [*102*] obtained for $SrFeO_{2.5}$ by TEM (right part [30],) and for the same section, reconstructed from 3D diffraction data on BM01A (left). The diffuse rods at (*h0l/2*) ± *β**b**** positions, are related to stacking faults of the tetrahedral layers as discussed in [30]; these can turn to become discrete satellite reflections with $\beta \approx$ ⅛ *or* ½, as a function of the sample history. The additional presumed superstructure reflections at (*h0l/4*) *or* (*h03/4l*) positions are diffuse rods related to the twin individuals with a common brownmillerite *b*-axis orientation, perpendicular to the present one. The right figure is reprinted with permission from [30]. Copyright 2008 American Chemical Society.

the common zone axis [*102*] seem to be almost identical, we underline that the degree of diffuse intensity is not only related to the sample history, but equally to the integration

limits for the reconstruction. Variations in the thickness of the integration layer of the (*hk¼*) plane, influences the appearance of diffuse scattering. This is related to contributions from different twin individuals, which are contributing in slightly different heights.

The results shown in figure 7 might suggest that BM01A should be regarded as a high performing 3D-TEM, at least for the diffraction part. The advantage for this in fact second generation synchrotron beamline is thereby, that all experiments are carried out at ambient conditions. This might become important when discussing non-stoichiometric oxides, as TEM experiments require ultra-high vacumn, which together with the reducing property of the e^--beam can result in severe stoichiometry problems.

A similar twinning scheme is obtained for the two intermediate phases, while $SrFeO_{2.75}$ with orthorhombic symmetry shows an equal amount of possible twin domains as $SrFeO_{2.5}$, i.e. 12 at maximum, while for $SrFeO_{2.875}$ the number gets reduced to six related to the tetragonal symmetry. The latter is even reduced to three, related to the centre of inversion present in the space group *I4/mmm*.

All reflections of any twin domain can be indexed in a $4\boldsymbol{a} \times 4\boldsymbol{a} \times 4\boldsymbol{a}$ supercell of the pseudo-cubic perovskite structure (see table S1 in the supplementary information (stacks.iop.org/JPhysD/48/504004/mmedia)), while the indexation of the respective (*hkl*) reflections for each phase are related by the relations given in table 2 with respect to the perovskite unit cell.

The results evidence that $SrFeO_{2.5}$ is, despite the stacking faults of the tetrahedral layers, still best described in the *Imma* space group, putting into question the results reported in [28, 29].

3.3. In situ oxidation of $SrFeO_{2.5}$ to $SrFeO_3$ followed up on BM01A

3.3.1. Single crystal in situ diffraction studies. Following up oxygen intercalation studies on single crystals at ambient temperature seems initially to be non-realistic; this is essentially related to the rather big size of oxygen ions ($r_{O^{2-}} = 1.4$ Å) combined with their two-fold negative charge, usually requiring elevated temperatures for oxygen diffusion to set in. The unusually high oxygen mobility found for some oxides with defect perovskite or K_2NiF_4 type frameworks already activated at ambient temperature, has been interpreted to rely on a phonon assisted diffusion mechanism [15, 31–41]. The applied electrochemical potential in a 1N KOH electrolyte is difficult to convert into an equivalent oxygen partial pressure. It must consequently be regarded as a useful synthesis tool, allowing us to reversibly intercalate oxygen ions, even up to important charge transfer rates. For the experiment we used an almost spherical $SrFeO_{2.5}$ crystal approximately 70 μm in diameter, which was found to get oxidized within a period of several days. As outlined in the experimental section, the crystal was glued with a silver glue on a 50 μm gold wire, thus presenting the working electrode, while a second 50 μm gold wire was used as the counter electrode and positioned in the electrolyte circuit close to the crystal. With respect to the low mass of the crystal, the current needed for complete oxidation in five days, lies in the picoampere region. We were however unable to oxidize spherical $SrFeO_{2.5}$ single crystals applying such low currents; this was probably due to complex over-potentials resulting in a too important amount of parasitic reactions. We therefore decided to operate with a continuously applied current of 10 μA, exceeding the theoretically calculated one by more than three orders of magnitude. In this way the reaction is no longer controlled by the flux of electrons as given in equation (1), but relies on the intercalation reaction kinetics only. That means the crystal reacts at maximum intercalation velocity, limited by its own reaction kinetics. This presents in principal a disadvantage as galvanostatic control is no longer achieved, but it guarantees on the other hand, a continuous oxidation on a kinetically controlled timescale. The phase analysis presented below is therefore done on a reaction time basis, rather than towards a defined oxygen stoichiometry correlated to the charge transfer. The reaction velocity is thus mainly determined by the size of the crystal, which for a diameter of 50–70 μm, was found to constitute several days, and which is very comfortable for a complete data collection.

As will be further outlined in detail below, following up the structural evolution is not as easy as for standard powder diffraction; this is related to the fact that the crystal used was twinned, resulting in four twin individuals. While on one hand this renders data analysis complex, on the other, it helps to differentiate the involved phases and to allow for following individual twin domain evolution.

3.3.2. Structural considerations and topochemical relations between $SrFeO_{2.5}$, $SrFeO_{2.75}$, $SrFeO_{2.875}$ and $SrFeO_3$. Since the oxygen stoichiometry in $SrFeO_{3-x}$ can also be reversibly controlled by electrochemical methods between $0 \leqslant x \leqslant 0.5$ at ambient temperature, and thus proceeding far from thermodynamical equilibrium, it is *a priori* questionable whether the same oxygen vacancy ordered phases can be obtained during a solid-state oxygen intercalation reaction performed at ambient temperature, compared to oxygen adjustment at elevated temperatures described in [27]. Room temperature reactions are kinetically controlled and thus proceed differently, compared to reactions carried out at elevated temperatures, where vacancy and related oxygen ordering are thermodynamically controlled.

Following up the oxygen intercalation into $SrFeO_{2.5}$ by *in situ* diffraction methods on single crystals, would therefore imply a series of advantages compared to *ex situ* characterization methods, but also compared to *in situ* powder diffraction. Accessing the whole reciprocal space would not only allow us to easily detect superstructure reflections related to oxygen ordering, but also to analyze diffuse scattering related to any type of disorder, including stacking faults. Despite these distinct advantages, the main drawback for *in situ* studies on single crystals is the strongly reduced reaction kinetics compared to polycrystalline powder samples, resulting in severe and uncontrolled mixing of different reaction intermediates during the reaction. Recent developments on single crystal diffraction using synchrotron radiation, essentially involving our ability to access a harmonics free primary beam together

with an ultra fast high resolution and almost background free area detectors, allow real time investigations today on single crystals in the frequency of a few min for a complete data collection even for crystals a few microns in size. This directly allows us to follow up a chemical reaction on single crystals, in a reasonable time window of a few min only. A major advantage compared to TEM is the fact that the studies here are carried out *in situ* under applied electrochemical potential and not under reducing conditions in a vacuum/e^--beam, while the whole reciprocal space becomes accessible under equilibrium conditions.

Coming to $SrFeO_{3-x}$, we used the *in situ* cell described in the experimental section for diffraction experiments under an applied electrochemical potential during the complete oxidation of $SrFeO_{2.5}$ to $SrFeO_3$. Besides our interest in following the structural evolution and formation of oxygen vacancy ordered intermediates, we were especially interested in the evolution of the microstructure and the disorder phenomena including stacking faults. Another point of interest concerns the evolution of domains in the course of the intercalation reaction. Starting from orthorhombic $SrFeO_{2.5}$, the symmetry changes for the reaction intermediates $SrFeO_{2.75}$ with orthorhombic symmetry and $SrFeO_{2.875}$ with tetragonal symmetry, would imply a complex domain structure, according to the fact that the starting compound is twinned as illustrated in figure 4, yielding four twin individuals. While $SrFeO_{2.75}$ with its orthorhombic symmetry and the *Cmmm* space group maintains the number of twin individuals of the starting crystal, $SrFeO_{2.875}$ with its tetragonal symmetry shows a maximum of six or respectively three individuals. The oxidation to the cubic perovskite-type structure results finally in only one domain structure.

Before entering the data analysis, we want to try to understand the oxygen intercalation mechanism following a topotactic reaction pathway, based on the structure models shown in figure 2. In this regard it seems reasonable to understand the formation of $SrFeO_{2.875}$ as a direct consequence of filling up regularly the oxygen vacancies along the 1D vacancy layer present in the brownmillerite framework. The tetrahedral layers are thus modified in a way as discussed for the homologous $SrCoO_{2.5}$ oxidation. Here the ordered intermediate phase $SrCoO_{2.875}$ as analyzed from *in situ* neutron diffraction [1], might be explained as the evolution of the former $(CoO_4)_\infty$ tetrahedral chains, towards a mixture of CoO_6 octahedra and Co_2O_9 square bi-pyramids. At the same time the octahedral layers remain basically unchanged. What is surprising for the $SrCoO_{3-x}$ system is the absence of a long range oxygen vacancy ordered $SrCoO_{2.75}$ phase. Unexpectedly, it shows instead an oxygen deficient perovskite type structure with cubic symmetry. This consequently implies that the oxygen intercalation mechanism into $SrCoO_{2.5}$ proceeds in a way, implying a rearrangement of all oxygen atoms on a local shell.

A similar and even more complex situation is present for the $SrFeO_{3-x}$ system. While the $SrFeO_{2.875}$ phase is fully equivalent to $SrCoO_{2.875}$, the $SrFeO_{2.75}$ shows an ordered $2a\sqrt{2} \times 2a \times a\sqrt{2}$ superstructure with respect to the parent perovskite. While a topotactic oxygen uptake from $SrFeO_{2.5}$ to $SrFeO_{2.875}$ appears to correspond to an oxygen intercalation reaction analogous to the $SrCoO_{3-x}$, this is no longer true for an oxygen uptake forming $SrFeO_{2.75}$. Starting from $SrFeO_{2.5}$, half of all FeO_6 octahedra and all FeO_4 tetrahedra get transformed towards Fe_2O_9 square bi-pyramids for $SrFeO_{2.75}$, implying an important restructuring of the octahedra and as well a tetrahedra sublattice. In this way the strong anisotropic character of the brownmillerite structure, established by an alternating octahedral and tetrahedral layer sequence, gets lost. Anisotropic oxygen diffusion in brownmillerite oxides has been evidenced e.g. for $CaFeO_{2.5}$ in [45]. Instead a more 3D network of corner-shared octahedra as well as octahedra/square-pyramids is established here. This implies consequently strong structural modifications on a local scale, which one may easily accept to proceed at elevated temperatures, but which might be questionable to understand for a reaction proceeding at ambient temperature. The formation of micro-domains as reported in [26] seems thus to be a plausible alternative in this case.

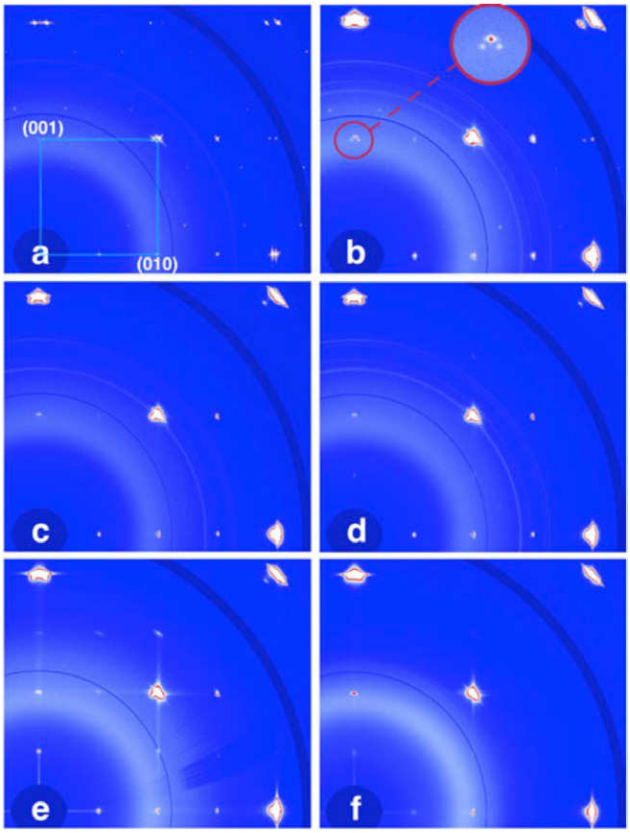

Figure 8. Evolution of the (*0kl*) plane during the electrochemical oxygen intercalation in $SrFeO_{2.5}$ (a) with the brownmillerite framework up to the cubic $SrFeO_3$ perovskite phase (f). The perovskite unit cell is outlined in (a). The insert in figure 8(b) shows the (*001*) reflection of the perovskite cell, corresponding to the (*201*)- and (*220*)-type reflections in the $SrFeO_{2.75}$ and $SrFeO_{2.875}$ phases respectively. The good spatial separation obtained by high-resolution synchrotron radiation is sufficient to separate between these two contributions allowing them to obtain and to follow their respective integral intensities with time.

3.3.3. Data analysis and reaction pathway. Figure 8 summarises all essential changes occurring for the (0*kl*) planes in the course of the electrochemical oxidation of $SrFeO_{2.5}$ with $a = 5.527(1)$ Å, $b = 15.59(2)$ Å and $c = 5.672(1)$ Å, related

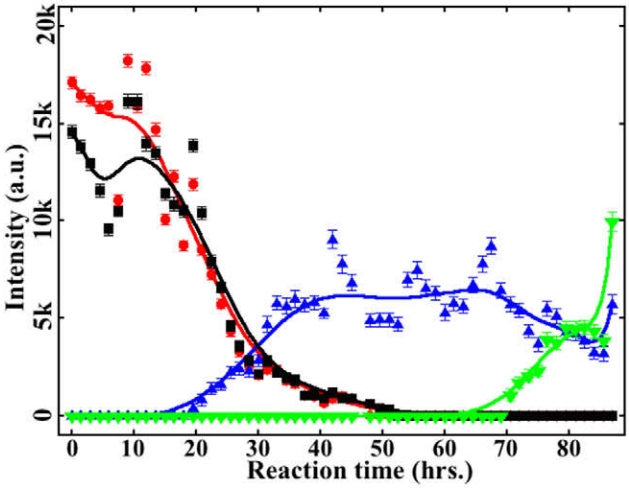

Figure 9. Evolution of the fractions of the different phases with time, obtained from intensities of respective reflections (all indexed with respect to the perovskite cell) during the electrochemical oxidation: ■ diffuse intensity (integrated on a fixed reciprocal lattice volume) taken from a constant volume along the rods in figure 5 for $SrFeO_{2.5;}$ ● presents the sum of the intensity of the two split (*001*) reflections of $SrFeO_{2.5}$ (see figure 8(b)); ▲ presents the intensity of the new (*001*) reflection of $SrFeO_{2.75}$ (which is in the course of oxidation mixed up together with $SrFeO_{2.875}$) and ▼ which corresponds to the intensity of the newly formed (*00½*) reflection, related to $SrFeO_{2.875}$ only. The final $SrFeO_3$ pattern shown in figure 8(f) has been obtained after three additional days of oxidation.

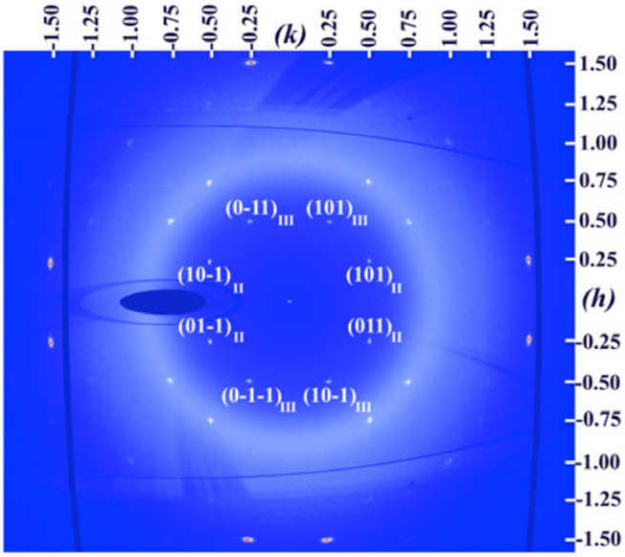

Figure 10. Reconstruction of the (*hk¼*) plane of the $SrFeO_{2.875}$ phase, obtained in the same orientation as for figure 6. The diffuse rods present in $SrFeO_{2.5}$ develop to sharp superstructure reflections for $SrFeO_{2.875}$, indicating long-range oxygen ordering upon electrochemical oxidation to get established. Contributions come from the twin individuals which already contributed to the diffuse rods in figure 6, here attributed to the twin individuals (II) and (III). Contributions from the newly formed twin domain (I) become easily obvious in figures 11(a) and (b) as they show a reduced intensity compared to the twin individuals present in the initial phase. We note that the central intensity does not correspond to an additional reflection but to a diffuse rod as illustrated in figure 8(e).

to the *Imma* space group. Figure 8(a) corresponds to the starting phase and shows the splitting of the (*00l*) reflections, separated by about 3° due to the twinning. The oxidation towards the $SrFeO_{2.75}$ phase with *Cmmm* symmetry and lattice parameters $a = 10.974(1)$ Å, $b = 7.702(1)$ Å and $c = 5.473(1)$ Å, leads to a strong reduction of the orthorhombicity, the *b*-axis corresponding to the former stacking axis of the brownmillerite framework, and taking $a_{\text{eff}} = 10.974/2$ Å.

The angular separation between the (*00l*) reflections can then be calculated to 0.15°, which corresponds exactly to what is observed when coming over figures 8(b) and (c), the latter essentially presenting the pure $SrFeO_{2.75}$ phase. The split (*001*) peak intensities decrease with the oxidation, while a new single reflection at a slightly higher $\boldsymbol{q}$-value develops. In detail, the disappearance of all brownmillerite reflections is, however, not perfectly realized, as we observe in figure 8(c) which shows a small amount of brownmillerite contributions such as the (*0½0*) reflection; we can rule out that these reflections belong to $SrFeO_{2.75}$, as no corresponding *d*-value exists for this phase. Figure 9 shows the evolution of the intensities of reflections and diffuse scattering with the reaction time. We see that the intensity of the diffuse rods shown in figure 5 decreases continuously with the intensity of the (*001*) reflection of the perovskite cell; this is equal to a (*101*)-type reflection of the brownmillerite phase. $SrFeO_{2.75}$ no longer shows the 1D diffuse rods as compared to the starting compound. Further oxidation then leads in figure 8(d) and more completely in figure 8(e) to the $SrFeO_{2.875}$ phase, which adopts *I4/mmm* symmetry and the associated lattice parameters of $a = 10.929(1)$ Å and $c = 7.698(1)$ Å. As further discussed below, this phase can in principal form three twin individuals, with the *c*-axis running into the three principal axes of the perovskite cell. We observed the appearance of diffuse lines along [*010*]/[*001*] around the (*011*)- and (*0½0*)-type perovskite reflections, while for the latter one, the diffuse lines reach quite low scattering angles, i.e. fairly high *d*-spacings. This type of diffuse scattering might be attributed to a correlation of planar defects, e.g. twin boundaries, which is probably related to the change in the twin structure, yielding twin domains with three different orientations of the tetragonal *c*-axis upon oxidation from $SrFeO_{2.75}$ to $SrFeO_{2.875}$. The uniform distribution of equivalent reflections in $SrFeO_{2.875}$ might be taken as a hint that one can assume the presence of microtwinning; this implies a small domain size for the different twin individuals together with an associated correlation length problem of as formed twin domains, which are responsible for the formation of the diffuse streaks. Similar diffuse lines have been found in $SrFeO_{3-x}$ thin-films [42–44], but which have been interpreted to probably rely on an inhomogeneous Sr/Fe concentration, which can be clearly excluded in our case. The creation of diffuse streaks just by changing the oxygen stoichiometry and the associated correlation problems of the as formed twin domains, might also present in the case of thin films a possible alternative interpretation. This is also a rather unique case, where diffuse streaks are induced by a change of oxygen stoichiometry, and related defects such as anti-phase boundaries, associated to the twin domain structure, can be controlled at ambient temperature.

The appearance of the (*00½*) reflection in figure 8(e) is another proof that the twin structure has changed, as a reaction pathway for oxygen intercalation with retention of the *b*-axis for the two brownmillerite twin sets, is incompatible with the formation of the (*00½*) reflection. This is justified for geometrical reasons, as the [*110*] direction of the $SrFeO_{2.875}$ phase is parallel to the [*010*] direction of the brownmillerite phase, resulting in an almost perfect equivalence of the (*110*) and (*020*) plane, comparing $SrFeO_{2.875}$ and $SrFeO_{2.5}$ respectively. This consequently implies that the (*½00*) and (*0½0*) reflections, i.e. the respective (*020*)-type reflections of the brownmillerite starting phase transform into the according (*110*)-type of the $SrFeO_{2.875}$ phase, while the third twin individual, at the (*00½*) reflection position of the perovskite cell, should not be formed, in case the underlying twin domain structure is preserved. The appearance of the new (*00½*) reflection thus evidences that the intercalation mechanism is changing the twin domain structure, which might originate from the specific structure of $SrFeO_{2.75}$.

As can be seen in figure 2, the structural evolution from $SrFeO_{2.5}$ to $SrFeO_{2.75}$ implies a considerable change of half of the former octahedra and all tetrahedra of the brownmillerite framework. While the formation of $SrFeO_{2.75}$ is still related to the given twin structure, i.e. maintaining the integrity of the initial orientation of the brownmillerite unit cell, this is no longer true when passing towards $SrFeO_{2.875}$. Given the defect structure of $SrFeO_{2.5}$, an evolution towards $SrFeO_{2.875}$ with a 3D connectivity of the FeO_6 octahedra, does therefore no longer imply the integrity of the underlying microstructure, i.e. the orientation of the former tetrahedral layers of the brownmillerite structure. In this regard it would be interesting to study if the electrochemically-obtained $SrFeO_{2.75}$ phase and twin structure, would yield again the native twin structure upon reduction to $SrFeO_{2.5}$.

The transformation towards the $SrFeO_{2.875}$ phase can be explicitly followed up with the evolution of the (*hk¼*) plane of the brownmillerite phase (see figures 6 and 10). Due to the twin structure of the starting phase, this plane shows initially only the scattering intensities in the form of diffuse rods, related to the stacking faults of the tetrahedral layers of $SrFeO_{2.5}$. Considering the 3D-microstructural evolution over $SrFeO_{2.75}$ towards $SrFeO_{2.875}$ as outlined above, one would consequently expect an evolution of the (*hk¼*) plane to develop exclusively reflections of the $SrFeO_{2.875}$ phase, which is effectively the case (see figure 10).

The reconstructed (*hk¼*) plane of $SrFeO_{2.875}$ shows weak but sharp superstructure reflections, only related to the long-range ordered oxygen vacancies for the different twin domains. This proves that long-range oxygen ordering is established during the oxygen intercalation reaction, and proceeds already at ambient temperature. It thus directly implies that oxygen is not only mobile in solid oxide frameworks, but is able to establish instantly, long-range correlations at an already ambient temperature. This is at first sight astonishing, taking into account the size and charge of the O^{2-} ions.

Figure 9 gives the intensity evolution with time of different reflections related to the specific phases encountered in course of the electrochemical oxidation of $SrFeO_{2.5}$. First

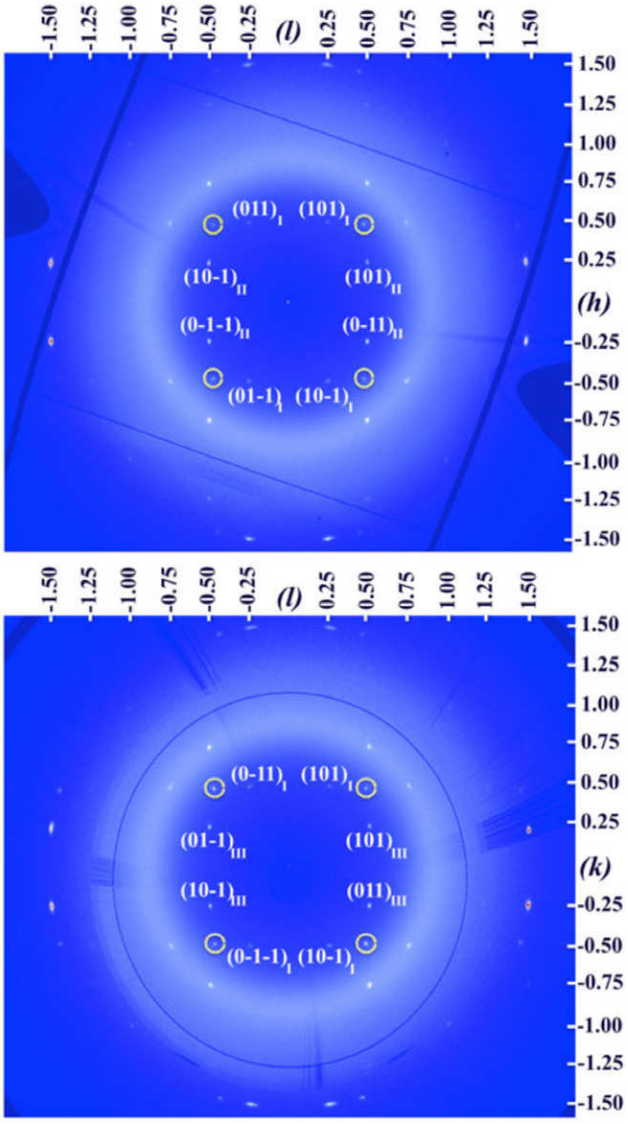

Figure 11. Reconstruction of the (*h¼l*) (top) and (*¼kl*) (bottom) plane containing the $SrFeO_{2.875}$ reflections. Indexations are given for the inner reflections with respect to the twin individuals (I) and (II) as well as (I) and (III). As becomes evident, the twin individual no. (I) shows a reduced intensity compared to the individuals nos. (II) and (III), which were already present as twin domains in the initial crystal, before no. (I) started to develop during the transition from $SrFeO_{2.75}$ to $SrFeO_{2.875}$. The reduced intensity can thus be explained statistically, related to a reduced probability during the formation of individual no. (I), transforming from the already existing domains (II) and (III). The yellow circles correspond to brownmillerite reflections, which did not completely disappear during the reaction and which can be indexed as (*011*)/(*110*)-type with a *d*-spacing of 5.19 Å, in the brownmillerite unit cell. We note the absence of these contributions in figure 10, which is related to the fact that twin individual no. (I) was absent in the initial starting phase. Note that for figures 10 and 11 the symmetry is not fourfold, as the zone axes of these planes correspond to the [*110*]-type directions of the tetragonal $SrFeO_{2.875}$ phase, going along with a 2/*m* symmetry.

the intensity of the diffuse rods present in $SrFeO_{2.5}$ decrease in the same way as the regular (*001*) reflection, while the new $SrFeO_{2.75}$ phase grows up, which can be seen from the new (*001*) reflection as shown in figures 8(a)–(f). Since almost all

reflections for $SrFeO_{2.75}$ and $SrFeO_{2.875}$ are superimposed, no reliable reflections originating from $SrFeO_{2.75}$ only could be identified. One support comes in this regard from the special twin structure, allowing us to attribute reflections such as (*00½*), to contribute exclusively to $SrFeO_{2.875}$. In this way we were able to distinguish between these two phases and to establish the phase sequence as summarized in figure 9.

The fact that the (*001*) $SrFeO_{2.75}$ reflection does not go down to zero is related to the fact that a contribution from $SrFeO_{2.875}$ is undiscernibly overlaid. For both the intermediate phases $SrFeO_{2.75}$ and $SrFeO_{2.875}$, the corresponding superstructure reflections have been found as expected from the structural models reported in [30]. This shows that complex oxygen ordering is possible in solid oxides already at ambient temperature.

4. Conclusion

In this study we investigated the electrochemical oxygen intercalation reaction into $SrFeO_{2.5}$ by *in situ* synchrotron diffraction on a single crystal on BM01A at the SNBL (ESRF), in a specially designed electrochemical cell. While this type of study carried out on polycrystalline samples has become a matter of routine, it is still a novelty when using single crystals and to the best of our knowledge, this is the first case where a complete solid-state reaction has been investigated to obtain 3D diffraction data obtained under *in situ* conditions. We not only demonstrated the feasibility of these types of experiments, but could also investigate microstructural aspects, which are simply not possible to obtain from powder diffraction methods. An important factor in successfully conducting this experiment is the performance of the diffractometer in terms of its primary beam quality and essentially the fast readout time of the quasi zero-noise detector.

In this context, a decisive point concerns the strongly enhanced sensitivity for weak superstructure reflections, which become easily accessible, while the same holds for diffuse intensities. Scanning up the whole reciprocal space then allows us to visualize at very high resolution even tiny details, which is of utmost importance, especially for reflection separation, e.g. for twin domains.

We could consequently confirm that long range oxygen ordering is established during the electrochemical oxygen intercalation reaction already at ambient temperature for the two reaction intermediates $SrFeO_{2.75}$ and $SrFeO_{2.875}$. Beyond this the analysis of the changes in the twin domain structure evidenced a topotactic reaction mechanism from $SrFeO_{2.5}$ to $SrFeO_{2.75}$, while the subsequent transition to $SrFeO_{2.875}$ yields surprisingly to a substantial modification of the microstructure, adding a third twin domain orientation along [*001*], which was absent before.

Oxygen intercalation reactions proceeding at ambient temperature thus not only allow us to show the complex structural changes involved in developing long range superstructures, but equally allow us to adjust the doping concentrations and the respective changes in the physical properties, which are interesting e.g. for the development of oxygen membranes and the related applications for energy materials. It might be equally interesting to modify the electronic properties, presently achieved by Sr-doping in perovskite-type oxides for spintronics. The fact that both Sr-doping of trivalent rare earth metals and oxygen intercalation result in hole-doping means that similar changes in the magnetic properties can be expected. Together with microstructural modifications of the twin structure, this might also allow us to yield new physical properties.

As a by-product of this study we could also reconfirm the ground state of $SrFeO_{2.5}$ to be described in the *Imma* space group, rather than in the *Pbma* and ordered $(FeO_4)_\infty$-tetrahedral chains together with a doubling of the *a*-axis parameter. In agreement with former TEM results [30], stacking disorder of the tetrahedral layers via diffuse scattering was confirmed here, qualifying BM01A to obtain results comparable to TEM, at least concerning the diffraction part.

While we have shown that solid-state reactions can in principle be observed on single crystals of a few μm in size, it becomes, however, clear that the complexity encountered in this study, e.g. describing the twin domain structure, shows that this approach is far from being used as a routine method. This remains true in spite of the results, which partially cannot be obtained from simple powder diffraction.

We are nevertheless convinced, that *in situ* single crystal diffraction offers huge potential to study non-stoichiometric compounds under *operando* conditions especially at ambient temperature; this will enable us to obtain structural information such as diffuse scattering and microstructural information related to domain effects such as twinning, far beyond that which standard powder diffraction allows us to obtain, which also holds for pair-distribution function analysis. This appears to be very promising not only for battery materials. In this context we want to underline, that the increasing performance especially of standard laboratory equipment, e.g. the use of μ-focus x-ray sources together with the availability of noise-free pixel detectors, allowing energy discrimination to minimize fluorescence, already present today a very promising avenue to explore chemical reactivity on μm sized single crystals.

Acknowledgments

This research was supported by the French National Research Agency through the project SECTOR (ANR-14-CE36-0006-01). We acknowledge the use of the synchrotron beam time on the BM01A diffractometer of the Swiss Norwegian beamline at the ESRF at Grenoble, France. We would also like to thank A da Silva (UM, ICGM, C2M) for the realization of the electrochemical cell used for *in situ* studies.

References

[1] Le Toquin R, Paulus W, Cousson A, Prestipino C and Lamberti C 2006 Time-resolved *in situ* studies of oxygen intercalation into $SrCoO_{2.5}$, performed by neutron diffraction and x-ray absorption spectroscopy *J. Am. Chem. Soc.* **128** 13161–74

[2] Courtney I A and Dahn J R 1997 Electrochemical and *in situ* x-ray diffraction studies of the reaction of lithium with tin oxide composites *J. Electrochem. Soc.* **144** 2045–52

[3] Legrand V, Merdrignac-Conanec O, Paulus W and Hansen T 2012 Study of the thermal nitridation of nanocrystalline $Ti(OH)_4$ by x-ray and *in situ* neutron powder diffraction *J. Phys. Chem.* A **116** 9561–7

[4] Kitaura R *et al* 2002 Formation of a 1D array of oxygen in a microporous metal-organic solid. *Science* **298** 2358–61

[5] Halder G J and Kepert C J 2005 *In situ* single-crystal x-ray diffraction studies of desorption and sorption in a flexible nanoporous molecular framework material *J. Am. Chem. Soc.* **127** 7891–900

[6] Miller S R, Wright P A, Devic T, Serre C, Férey G, Llewellyn P L, Denoyel R, Gaberova L and Filinchuk Y 2009 Single crystal x-ray diffraction studies of carbon dioxide and fuel-related gases adsorbed on the small pore scandium terephthalate metal organic framework, $Sc_2(O_2CC_6H_4CO_2)_3$ *Langmuir* **25** 3618–26

[7] BM01A (www.esrf.eu/UsersAndScience/Experiments/CRG/BM01/bm01-a)

[8] Ceretti M, Piovano A, Cousson A, Berthier T, Meven M, Agostini G, Schefer J, Hernandez O, Lamberti O and Paulus W 2012 Growth and characterization of large high quality Bownmillerite $CaFeO_{2.5}$ single crystals *Cryst. Eng. Comm.* **14** 5771–6

[9] Maljuk A, Lebon A, Damljanović V, Ulrich C, Lin C T, Adler P and Keimer B 2006 Growth and oxygen treatment of $SrFeO_{3-y}$ single crystals *J. Cryst. Growth* **291** 412–5

[10] Watanabe H 1957 Magnetic properties of Perovskites containing strontium I. strontium-rich ferrites and cobaltites *J. Phys. Soc. Japan* **12** 515–22

[11] Gallagher P K, MacChesney J B and Buchanan D N E 1964 Mössbauer effect in the system $SrFeO_{2.5-3.0}$ *J. Chem. Phys.* **41** 2429–34

[12] Grenier J-C, Ea N, Pouchard M and Hagenmuller P 1985 Structural transitions at high temperature in $Sr_2Fe_2O_5$ *J. Solid State Chem.* **58** 243–52

[13] Adler P, Schwarz U, Syassen K, Milner A P, Pasternak M P and Hanfland M 2000 Structural phase transitions in $Sr_2Fe_2O_5$ under high pressure *J. Solid State Chem.* **155** 381–8

[14] Kozhevnikov V L, Leonidov I A, Patrakeev M V, Mitberg E B and Poeppelmeier K R 2001 Electrical properties of the ferrite $SrFeO_y$ at high temperatures *J. Solid State Chem.* **158** 320–6

[15] Kawakami T, Nasu S, Kuzushita K, Sasaki T, Morimoto S, Yamada T, Endo S, Kawasaki S and Takano M 2003 High-pressure Mössbauer and x-ray powder diffraction studies of $SrFeO_3$ *J. Phys. Soc. Japan* **72** 33–6

[16] Greaves C, Jacobson A J, Tofield B C and Fender B E F 1975 A powder neutron diffraction investigation of the nuclear and magnetic structure of $Sr_2Fe_2O_5$ *Acta Crystallogr.* B **31** 641–6

[17] Gibb T C 1985 Magnetic exchange interactions in perovskite solid solutions. Part 5. The unusual defect structure of $SrFeO_{3-y}$ *J. Chem. Soc. Dalt. Trans.* **7** 1455

[18] Grenier J-C, Wattiaux A, Doumerc J-P, Dordor P, Fournes L, Chaminade J-P and Pouchard M 1992 Electrochemical oxygen intercalation into oxide networks *J. Solid State Chem.* **96** 20–30

[19] Lebon A, Adler P, Bernhard C, Boris A V, Pimenov A V, Maljuk A, Lin C T, Ulrich C and Keimer B 2004 Magnetism, charge order, and giant magnetoresistance in $SrFeO_{3-\delta}$ single crystals *Phys. Rev. Lett.* **92** 037202

[20] Ishiwata S, Tokunaga M, Kaneko Y, Okuyama D, Tokunaga Y, Wakimoto S, Kakurai K, Arima T, Taguchi Y and Tokura Y 2011 Versatile helimagnetic phases under magnetic fields in cubic perovskite $SrFeO_3$ *Phys. Rev.* B **84** 054427

[21] Reehuis M, Ulrich C, Maljuk A, Niedermayer C, Ouladdiaf B, Hoser A, Hofmann T and Keimer B 2012 Neutron diffraction study of spin and charge ordering in $SrFeO_{3-\delta}$ *Phys. Rev.* B **85** 184109

[22] Takeda T, Yamaguchi Y and Watanabe H 1972 Magnetic structure of $SrFeO_3$ *J. Phys. Soc. Japan* **33** 967–9

[23] Tsujimoto Y, Tassel C, Hayashi N, Watanabe T, Kageyama H, Yoshimura K, Takano M, Ceretti M, Ritter C and Paulus W 2007 Infinite-layer iron oxide with a square-planar coordination *Nature* **450** 1062–5

[24] Takeda Y, Kanno K, Takada T, Yamamoto O, Takano M, Nakayama N and Bando Y 1986 Phase relation in the oxygen nonstoichiometric system, $SrFeO_x$ ($2.5 \leqslant x \leqslant 3.0$) *J. Solid State Chem.* **63** 237–49

[25] Takano M, Okita T, Nakayama N, Bando Y, Takeda Y, Yamamoto O and Goodenough J B 1988 Dependence of the structure and electronic state of $SrFeO_x$ ($2.5 \leqslant x \leqslant 3$) on composition and temperature *J. Solid State Chem.* **73** 140–50

[26] Nemudry A, Weiss M, Gainutdinov I, Boldyrev V and Schöllhorn R 1998 Room Temperature electrochemical redox reactions of the defect perovskite $SrFeO_{2.5+x}$ *Chem. Mater.* **10** 2403–11

[27] Hodges J P, Short S, Jorgensen J D, Xiong X, Dabrowski B, Mini S M and Kimball C W 2000 Evolution of oxygen-vacancy ordered crystal structures in the perovskite series $Sr_nFe_nO_{3n-1}$ ($n = 2$, 4, 8, and ∞), and the relationship to electronic and magnetic properties *J. Solid State Chem.* **151** 190–209

[28] Auckett J E, Studer A J, Sharma N and Ling C D 2012 Floating-zone growth of brownmillerite $Sr_2Fe_2O_5$ and the observation of a chain-ordered superstructure by single-crystal neutron diffraction *Solid State Ion.* **225** 432–6

[29] Auckett J E, Studer A J, Pellegrini E, Ollivier J, Johnson M R, Schober H, Miiller W and Ling C D 2013 Combined experimental and computational study of oxide ion conduction dynamics in $Sr_2Fe_2O_5$ Brownmillerite *Chem. Mater.* **25** 3080–7

[30] D'Hondt H, Abakumov A M, Hadermann J, Kalyuzhnaya A S, Rozova M G, Antipov E V. and Van Tendeloo G 2008 Tetrahedral chain order in the $Sr_2Fe_2O_5$ Brownmillerite *Chem. Mater.* **20** 7188–94

[31] Paulus W, Schober H, Eibl S, Johnson M, Berthier T, Hernandez O, Ceretti M, Plazanet M, Conder K and Lamberti C 2008 Lattice dynamics to trigger low temperature oxygen mobility in solid oxide ion conductors *J. Am. Chem. Soc.* **130** 16080–5

[32] Piovano A, Agostini G, Frenkel A I, Bertier T, Prestipino C, Ceretti M, Paulus W and Lamberti C 2011 Time resolved *in situ* XAFS study of the electrochemical oxygen intercalation in $SrFeO_{2.5}$ Brownmillerite structure: comparison with the homologous $SrCoO_{2.5}$ system *J. Phys. Chem.* C **115** 1311–22

[33] Gupta K, Singh S, Ceretti M, Rao M S R and Paulus W 2013 Scaling of extended defects in nano-sized Brownmillerite $CaFeO_{2.5}$ *Phys. Status Solidi* A **210** 1771–7

[34] Perrichon A, Piovano A, Boehm M, Zbiri M, Johnson M, Schober H, Ceretti M and Paulus W 2015 Lattice dynamics modified by excess oxygen in $Nd_2NiO_{4+\delta}$: triggering low-temperature oxygen diffusion *J. Phys. Chem.* C **119** 1557–64

[35] Piovano A, Ceretti M, Johnson M R, Agostini G, Paulus W and Lamberti C 2015 Anisotropy in the Raman scattering of a $CaFeO_{2.5}$ single crystal and its link with oxygen ordering in Brownmillerite frameworks *J. Phys.: Condens. Matter* **27** 225403

[36] Corallini S *et al* 2015 1D oxygen diffusion mechanism in Sr_2ScGaO_5 electrolyte explored by neutron and synchrotron diffraction, ^{17}O NMR, and density functional theory calculations *J. Phys. Chem.* C **119** 11447–58

[37] Paulus W, Cousson A, Dhalenne G, Berthon J, Revcolevschi A, Hosoya S, Treutmann W, Heger G and Le Toquin R 2002 Neutron diffraction studies of stoichiometric and oxygen intercalated La_2NiO_4 single crystals *Solid State Sci.* **4** 565–73

[38] Le Dréau L, Prestipino C, Hernandez O, Schefer J, Vaughan G, Paofai S, Perez-Mato J M, Hosoya S and Paulus W 2012 Structural modulation and phase transitions in $La_2CoO_{4.14}$ investigated by synchrotron x-ray and neutron single-crystal diffraction *Inorg. Chem.* **51** 9789–98

[39] Villesuzanne A, Paulus W, Cousson A, Hosoya S, Le Dréau L, Hernandez O, Prestipino C, Ikbel Houchati M and Schefer J 2010 On the role of lattice dynamics on low-temperature oxygen mobility in solid oxides: a neutron diffraction and first-principles investigation of $La_2CuO_{4+\delta}$ *J. Solid State Electrochem.* **15** 357–66

[40] Houchati M I, Ceretti M, Ritter C and Paulus W 2012 From T to T′-La_2CuO_4 via oxygen vacancy ordered $La_2CuO_{3.5}$ *Chem. Mater.* **24** 3811–5

[41] Bassat J-M, Burriel M, Wahyudi O, Castaing R, Ceretti M, Veber P, Weill I, Villesuzanne A, Grenier J-C, Paulus W and Kilner J A 2013 Anisotropic oxygen diffusion properties in $Pr_2NiO_{4+\delta}$ and $Nd_2NiO_{4+\delta}$ single crystals *J. Phys. Chem.* C **117** 26466–72

[42] Solís C, Rossell M D, Garcia G, Figueras A, Van Tendeloo G and Santiso J 2008 Microstructure and high temperature transport properties of high quality epitaxial $SrFeO_{3-\delta}$ films *Solid State Ion.* **179** 1996–9

[43] Lebedev O I, Verbeeck J, Van Tendeloo G, Hayashi N, Terashima T and Takano M 2004 Structure and microstructure of epitaxial $SrnFenO_{3n-1}$ films *Phil. Mag.* **84** 3825–41

[44] Tofield B C, Greaves C and Fender B E F 1975 The $SrFeO_{2.5}$ | $SrFeO_{3.0}$ system. evidence of a new phase $Sr_4Fe_4O_{11}$ ($SrFeO_{2.75}$) *Mater. Res. Bull.* **10** 737–45

[45] Inoue S, Kawai M, Ichikawa N, Kageyama H, Paulus W and Shimakawa Y 2010 Anisotropic oxygen diffusion at low temperature in perovskite-structure iron oxides *Nat. Chem.* **2** 213–7